

Studies of Vector Boson Scattering And Triboson Production with DELPHES Parametrized Fast Simulation for Snowmass 2013

C. Degrande^a, J. L. Holzbauer^b, S.-C. Hsu^c, A. V. Kotwal^d, S. Li^d,
M. Marx^c, O. Mattelaer^a, J. Metcalfe^e, M.-A. Pleier^e, C. Pollard^d,
M. Rominsky^f, D. Wackerth^g

^a*University of Illinois at Urbana-Champaign*

^b*University of Mississippi*

^c*University of Washington*

^d*Duke University*

^e*Brookhaven National Laboratory*

^f*Fermi National Accelerator Laboratory*

^g*University at Buffalo, the State University of New York*

June 8, 2018

Abstract

Multiboson production provides a unique way to probe Electroweak Symmetry Breaking (EWSB) and physics beyond the Standard Model (SM). With the discovery of the Higgs boson, the default model is that EWSB occurs according to the Higgs mechanism. Deviations from the SM in Higgs and gauge boson properties due to new physics at a higher energy scale can be parameterized by higher-dimension operators in an Effective Field Theory (EFT). We present sensitivity studies for dimension-6 and dimension-8 operators in an EFT by looking for anomalous vector boson scattering and triboson production, at proton-proton colliders with center-of-mass energies of 14 TeV, 33 TeV and 100 TeV, respectively.

1 Introduction

Multiboson production provides a unique way to probe Electroweak Symmetry Breaking (EWSB) and physics beyond the Standard Model (SM). With the discovery of the Higgs boson, the default model is that EWSB occurs according to the Higgs mechanism. In this case, all the couplings are completely specified. The gauge and Higgs sectors of the SM can be probed by studying vector boson scattering (VBS) and triboson production. These processes provide unique probes of quartic couplings which to date have not been studied extensively, since past experiments were mostly sensitive to diboson production. Deviations from SM predictions will give clues to physics beyond the SM.

Assuming that the energy scale associated with this new physics is sufficiently high compared to the masses of the gauge and Higgs bosons, we are motivated to use Effective Field Theory [1] to parameterize the new physics in channels involving these particles. The truncated EFT Lagrangian employed in our study is

$$\mathcal{L} = \mathcal{L}^{SM} + \sum_i \frac{c_i}{\Lambda^2} \mathcal{O}_i + \sum_j \frac{f_j}{\Lambda^4} \mathcal{O}_j \quad (1)$$

where \mathcal{O}_i and \mathcal{O}_j are the dimension-6 and dimension-8 operators [2] respectively, and c_i and f_j represent the numerical coefficients associated with these operators. These operators are induced by integrating out the new degrees of freedom, and the numerical coefficients are meant to be derivable from a more complete high-energy theory. Λ is a mass-dimension parameter associated with the energy scale of the new degrees of freedom which have been integrated out.

We choose operators that are Lorentz-invariant and gauge-invariant under the SM electroweak group $SU(2)_L \times U(1)_Y$, and contain the electroweak gauge and Higgs fields. Thus, EWSB is induced only by the spontaneous symmetry breaking as in the SM, due to the Higgs vacuum expectation value, and there is no explicit breaking of electroweak symmetry. This latter point is one of the differences between this EFT expansion and the traditional method of anomalous couplings where some operators explicitly break gauge invariance.

For this study, we tested both dimension-6 operators and dimension-8 operators at pp colliders with $\sqrt{s} = 14, 33$ and 100 TeV. This Snowmass exercise was performed using MADGRAPH [3] for event generation with CTEQ6L1 [4] PDF set, PYTHIA for showering and a special version of DELPHES [5] for the detector simulation. The effect of multiple interactions at high instantaneous luminosity was simulated using specially designed pileup files [6, 7, 8].

For the vector boson scattering process, we have chosen to study the fully-leptonic decay channels of the ZZ , WZ and same-sign WW final states. These final states do not suffer from large $t\bar{t}$ backgrounds. For the triboson final states involving heavy gauge bosons, we have chosen the fully-leptonic WWW final state because it has the largest production cross section \times branching ratio compared to all other combinations of heavy gauge bosons, and is separable from diboson backgrounds. We have also studied the photonic channels using the $Z\gamma\gamma$ final state.

2 VBS $ZZ \rightarrow 4\ell$

In this vector boson scattering channel, we explore anomalous production by studying the invariant mass distribution of the ZZ diboson pair. New physics is parameterized by the following dimension-6 operator

$$\mathcal{L}_{\phi W} = \frac{c_{\phi W}}{\Lambda^2} \text{Tr}(W^{\mu\nu} W_{\mu\nu}) \phi^\dagger \phi \quad (2)$$

or by one of the dimension-8 operators

$$\begin{aligned} \mathcal{L}_{T,8} &= \frac{f_{T8}}{\Lambda^4} B_{\mu\nu} B^{\mu\nu} B_{\alpha\beta} B^{\alpha\beta} \\ \mathcal{L}_{T,9} &= \frac{f_{T9}}{\Lambda^4} B_{\alpha\mu} B^{\mu\beta} B_{\beta\nu} B^{\nu\alpha} \end{aligned} \quad (3)$$

where ϕ is the SM Higgs field, and $W^{\mu\nu}$ ($B^{\mu\nu}$) are the field strength tensors derived from the $SU(2)_L$ ($U(1)_Y$) gauge fields. The fully-leptonic VBS $ZZ \rightarrow 4\ell$ channel provides a fully reconstructible ZZ final state with small mis-identification backgrounds [9] which can be neglected in this sensitivity study. The contribution from non-VBS diboson production accompanied by QCD jets is reduced by requiring the forward jet-jet mass to be greater than 1 TeV, and the surviving background is included in this study.

The operator $\mathcal{L}_{\phi W}$ was chosen for this study based on comparing cross section enhancements due to individual dimension-6 operators with their coefficients set to a non-zero, nominal value. This operator was found to give the largest enhancement. Similar comparisons of cross section enhancements due to individual dimension-8 operators were also performed and are shown in Table 10. The $\mathcal{L}_{T,0}$ and $\mathcal{L}_{T,1}$ operators give the largest enhancement, followed by $\mathcal{L}_{T,2}$, $\mathcal{L}_{T,8}$ and $\mathcal{L}_{T,9}$. The first three of these operators contain the same field strength tensors, and the study of $\mathcal{L}_{T,1}$ using the VBS WZ final state is presented in the next section. For the VBS ZZ final state, we chose the dimension-8 operators in Eqn. 3 because they involve only the electrically-neutral gauge fields and can be probed by the ZZ final state but not the WZ or WW final states.

MADGRAPH 5.1.5.10 is used for the generation of VBS ZZ (SM) and non-VBS (SM ZZ QCD) processes as well as the non-SM processes mentioned above. Z bosons were required to decay to electron or muon pairs.

2.1 Event Selection

After PYTHIA 6.4 [10] parton showering, additional detector effects are applied using DELPHES 3.0.9 [11] with the Snowmass parameterization [6, 7, 8]. Candidate VBS ZZ events are selected according to the following criteria:

- Exactly four selected leptons (each with $p_T > 25$ GeV) which can be separated into two opposite sign, same flavor pairs (No Z mass window requirement)
- At least two selected jets, each with $p_T > 50$ GeV
- $m_{jj} > 1$ TeV, where m_{jj} is the invariant mass of the two highest- p_T selected jets

2.2 Statistical Analysis

To determine the expected sensitivity to beyond-SM (BSM) ZZ contribution, the background-only p_0 -value expected for signal+background is calculated using the $m_{4\ell}$ spectrum. In order to show the improvement possible with the increased luminosity and center-of-mass energy, the 5σ discovery potential and 95% CL limits are studied. Since the 4-lepton mass is the process $\sqrt{\hat{s}}$, the study of its distribution directly probes the energy-dependence of the new physics.

At sufficiently high energy, the amplitude predicted by higher-dimension operators will eventually violate unitarity. In this regime, the new physics that presumably restores unitarity is expected to be probed directly, such as the production of on-shell resonances. This is a very interesting regime because the masses and couplings of new resonances can be measured independently, which is a much more powerful probe as compared to the low-energy regime where only the appropriate ratio of coupling and mass can be probed. Furthermore, in the high energy regime it is also possible to study new decay modes of the resonances, whereas in the low-energy regime of EFT applicability we can only study the anomalous production of SM particles. The regime above the unitarity bound is probed more strongly by the higher energy colliders.

We present the sensitivity to the higher-dimension operators in two ways. In the first case, we assume that new physics is only probed “virtually” by higher-dimension operators involving SM fields, and we require the generated events to lie below the unitarity bound in the diboson mass. In the second case, we allow the collider to probe the sensitivity to new physics above the unitarity bound through direct production of new resonances and measuring their masses, couplings and decay branching ratios. Since an ultraviolet-complete theory of strongly-interacting electroweak sector is not available for the additional physics that would be accessible in this high-energy regime, as a proxy we also quote the sensitivity to the higher-dimension operators without making the unitarity bound requirement on the diboson mass.

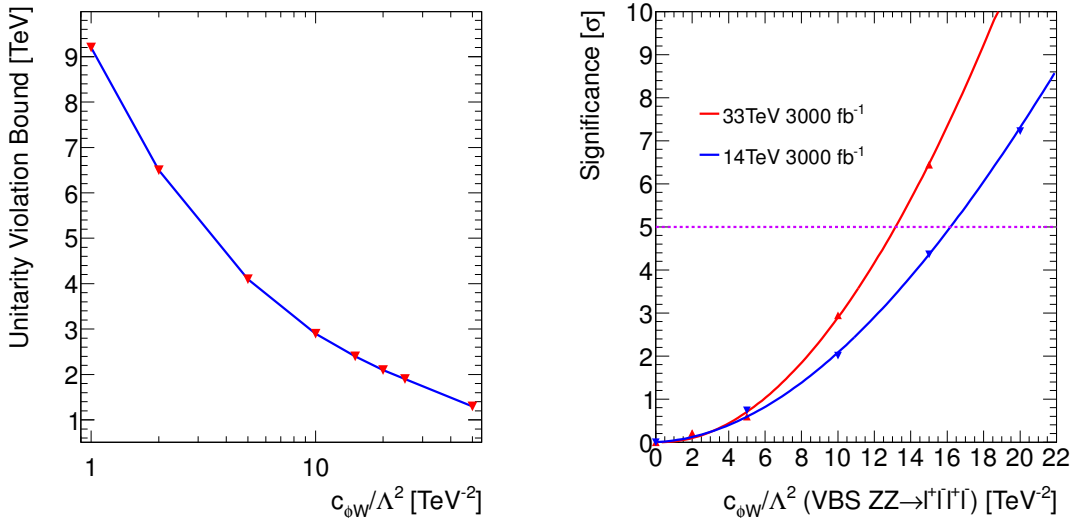


Figure 1: The unitarity violation bounds (left) and signal significances (right) are shown as a function of dimension-6 operator $c_{\phi W}/\Lambda^2$ coefficient values in $pp \rightarrow ZZ + 2j \rightarrow 4\ell + 2j$ processes. The UV bounds are not applied in the significance plot.

The unitarity violation (UV) bounds are calculated using the form factor tool available with VBFNLO [12]. The bounds, which are shown in the left plots of Figure 1 and Figure 2, vary as a function of the coefficients of the higher-dimension operators. One method of imposing unitarity preservation is to apply the UV bound as an upper bound on the invariant mass of the final-state bosons at truth-level. We use this method through this study. As expected, when the coefficients approach zero the bound goes to infinity, since the SM amplitude respects unitarity at all energies.

Application of the bound lowers the sensitivity of the search, especially when the coefficient is large. We present the 5σ -significance discovery values and 95% CL limits with and without applying the UV bound in Table 1. The reconstructed 4-lepton invariant mass distributions are shown in Figure 3 and Figure 4 without and with the UV bound, respectively. The right plots of Figure 1 and Figure 2 show the signal significance as a function of f_{T8}/Λ^4 , f_{T9}/Λ^4 and $c_{\phi W}/\Lambda^2$ without the UV bound applied.

Parameter	Luminosity [fb ⁻¹]	14 TeV		33 TeV	
		5 σ	95% CL	5 σ	95% CL
$c_{\phi W}/\Lambda^2$ [TeV ⁻²]	3000	16.2 (16.2)	9.7 (9.7)	13.2 (13.2)	8.2 (8.2)
	300	31.3 (31.5)	18.2 (18.3)	23.8 (23.8)	14.7 (14.7)
f_{T8}/Λ^4 [TeV ⁻⁴]	3000	2.9 (4.7)	1.7 (2.4)	1.6 (1.7)	1.0 (1.3)
	300	5.5 (8.4)	3.2 (5.3)	2.8 (2.3)	1.8 (1.8)
f_{T9}/Λ^4 [TeV ⁻⁴]	3000	5.7 (6.3)	3.9 (4.6)	3.8 (6.6)	2.5 (3.5)
	300	8.7 (9.0)	6.2 (6.7)	6.3 (10.1)	4.2 (8.2)

Table 1: In $pp \rightarrow ZZ + 2j \rightarrow 4\ell + 2j$ processes, 5σ -significance discovery values and 95% CL limits are shown for coefficients of high-dimension operators with 300 fb⁻¹/3000 fb⁻¹ of integrated luminosity. To show the impact of the UV bound, the corresponding results are shown in parentheses.

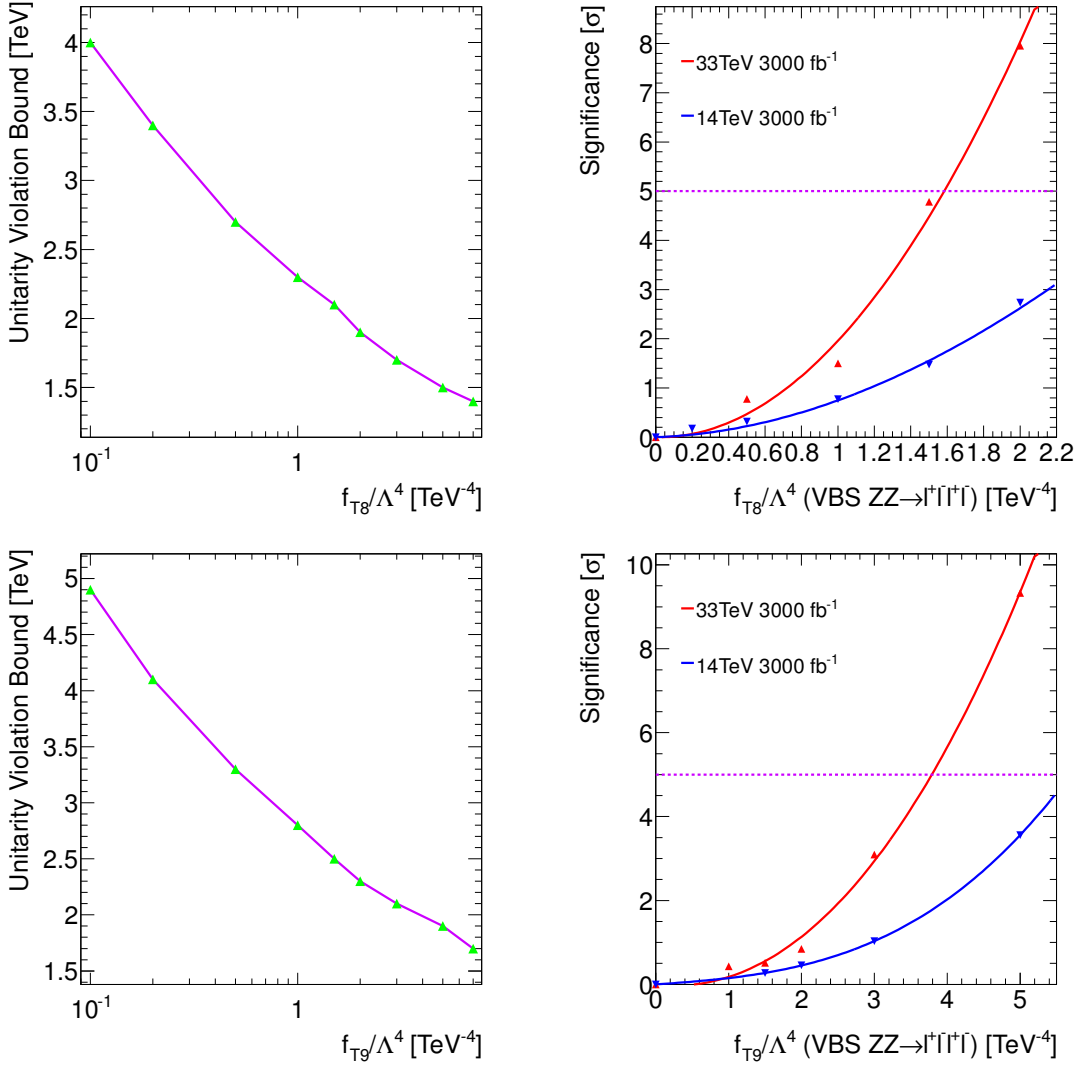


Figure 2: The unitarity violation bounds (left) and signal significances (right) are shown as a function of dimension-8 operator $\mathcal{L}_{T,8}$ (top) and $\mathcal{L}_{T,9}$ (bottom) coefficient values in $pp \rightarrow ZZ + 2j \rightarrow 4\ell + 2j$ processes. The UV bounds are not applied in the significance plots.

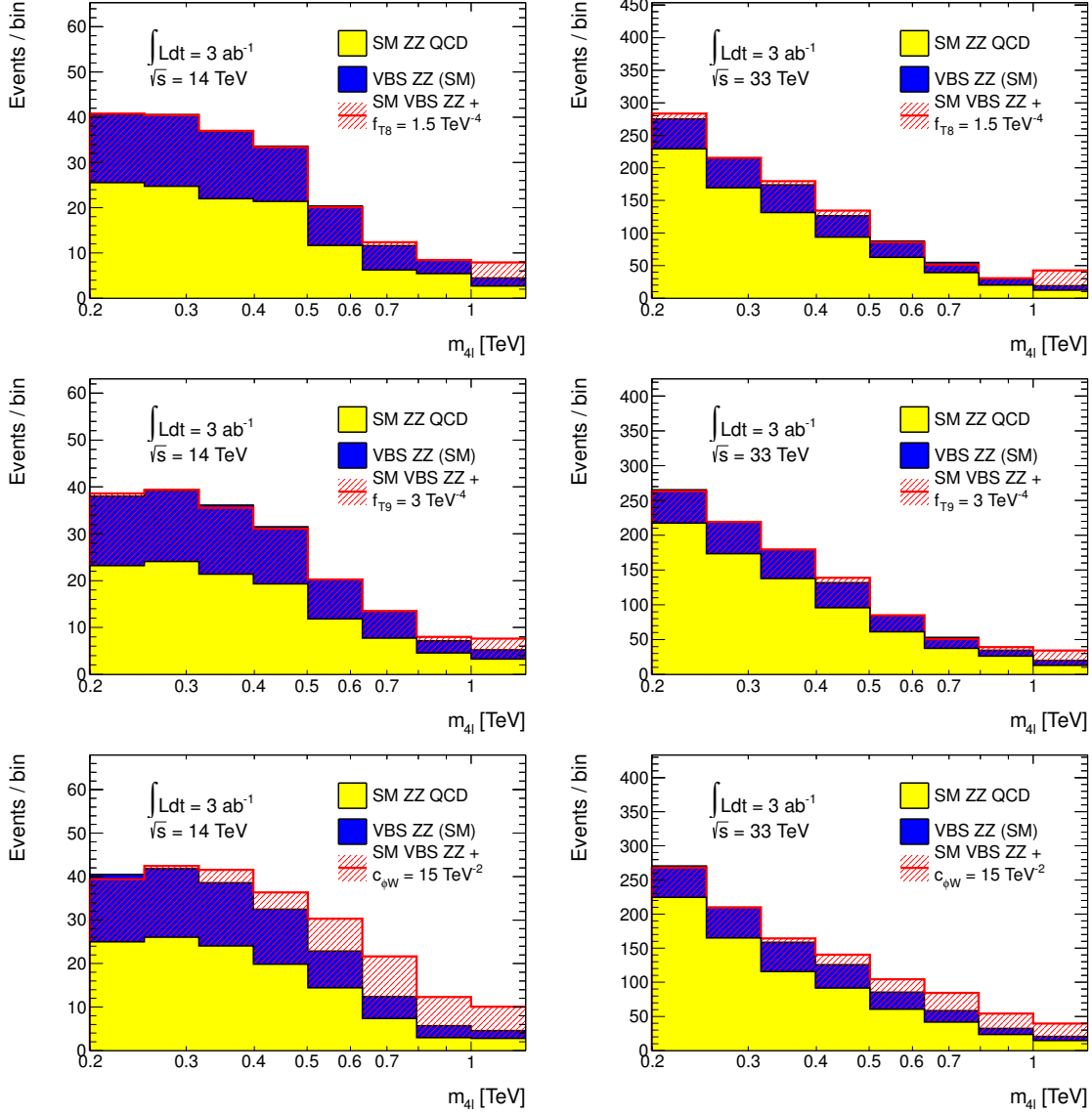


Figure 3: In the $pp \rightarrow ZZ + 2j \rightarrow 4\ell + 2j$ process, the reconstructed 4-lepton mass ($m_{4\ell}$) spectrum comparisons between Standard Model and dimension-8 operator coefficient $f_{T8}/\Lambda^4 = 1.5 \text{ TeV}^{-4}$ (top), $f_{T9}/\Lambda^4 = 3 \text{ TeV}^{-4}$ (middle) and dimension-6 operator coefficient $c_{\phi W}/\Lambda^2 = 15 \text{ TeV}^{-2}$ (bottom) are shown after requiring $m_{jj} > 1 \text{ TeV}$ at $\sqrt{s} = 14 \text{ TeV}$ (left) and 33 TeV (right). The overflow and underflow bins are included in the plots. The UV bound is not applied.

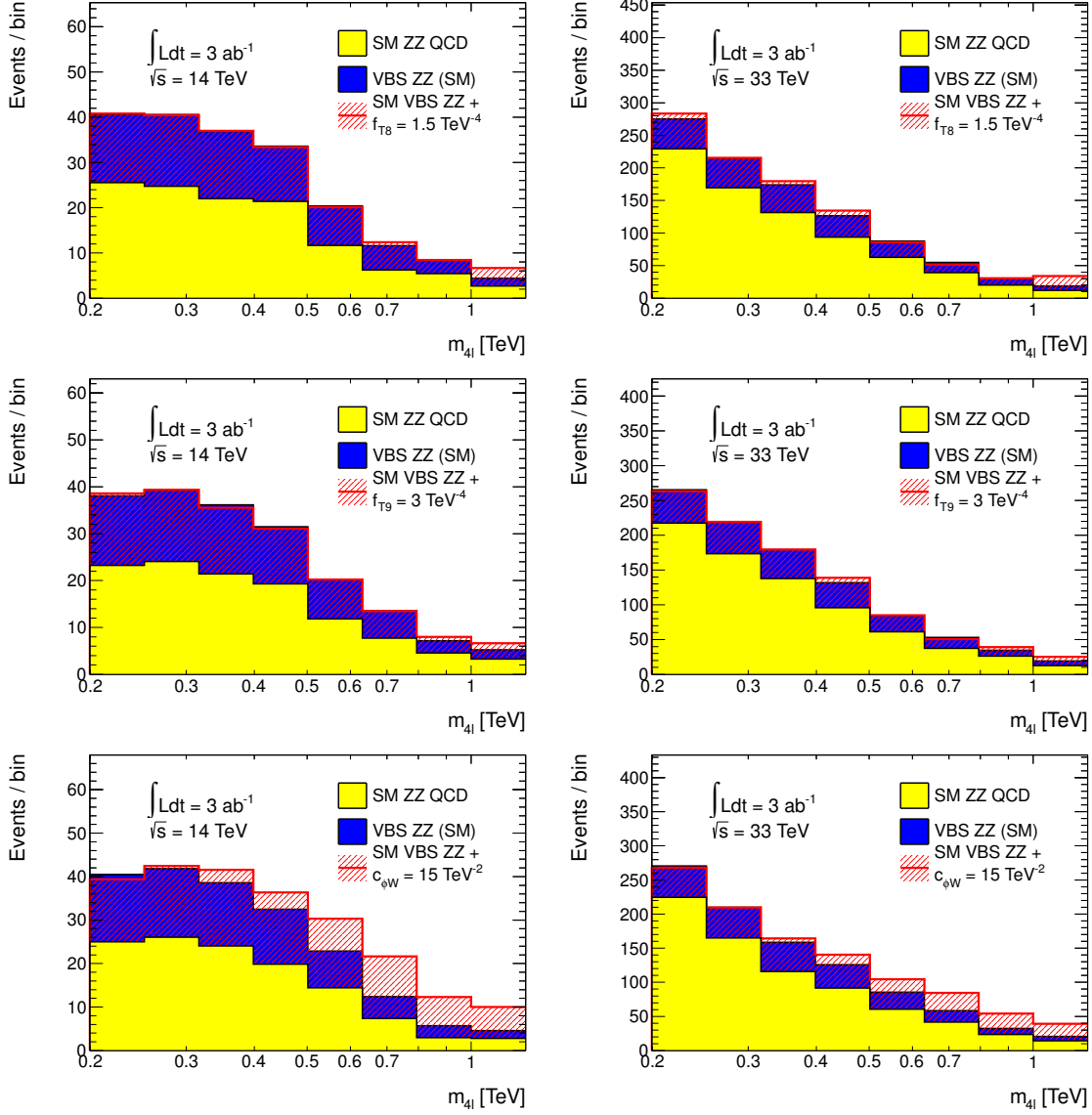


Figure 4: In the $pp \rightarrow ZZ + 2j \rightarrow 4\ell + 2j$ process, the reconstructed 4-lepton mass ($m_{4\ell}$) spectrum comparisons between Standard Model and dimension-8 operator coefficient $f_{T8}/\Lambda^4 = 1.5 \text{ TeV}^{-4}$ (top), $f_{T9}/\Lambda^4 = 3 \text{ TeV}^{-4}$ (middle) and dimension-6 operator coefficient $c_{\phi W}/\Lambda^2 = 15 \text{ TeV}^{-2}$ (bottom) are shown after requiring $m_{jj} > 1 \text{ TeV}$ at $\sqrt{s} = 14 \text{ TeV}$ (left) and 33 TeV (right). The overflow and underflow bins are included in the plots. The UV bound is applied.

3 VBS $WZ \rightarrow \ell\nu\ell\ell$

We parameterize new physics in this channel using the dimension-8 operator

$$\mathcal{L}_{T,1} = \frac{f_{T1}}{\Lambda^4} \text{Tr}[\hat{W}_{\alpha\nu}\hat{W}^{\mu\beta}] \times \text{Tr}[\hat{W}_{\mu\beta}\hat{W}^{\alpha\nu}] \quad (4)$$

and dimension-6 operator

$$\mathcal{L}_{\phi d} = \frac{c_{\phi d}}{\Lambda^2} \partial_\mu(\phi^\dagger\phi)\partial^\mu(\phi^\dagger\phi) \quad (5)$$

As shown in Table 9, the $\mathcal{L}_{T,1}$ operator produces the largest cross section enhancement for the VBS WZ final state. The $\mathcal{L}_{\phi d}$ operator is chosen because its coefficient can be easily translated into a modification of the Higgs boson couplings to SM particles. Therefore this operator provides a way to tune the $\phi \rightarrow WW$ and $\phi \rightarrow ZZ$ couplings and check the impact on unitarity violation in the VBS process if the Higgs couplings deviated from the SM.

The fully leptonic VBS $WZ \rightarrow \ell\nu\ell\ell$ channel can be reconstructed by solving for the neutrino p_z using the W boson mass constraint. Its cross section is larger than that of VBS $ZZ \rightarrow 4\ell$ and it can probe some operators better than the latter process. The electron and muon decay channels are used in this study. Mis-identification backgrounds are small in this channel, as shown in [13] and therefore neglected in this sensitivity study. The lepton from the W boson decay must be identified in order to use the W mass constraint. The procedure described in [14, 15] is also used here.

Non-VBS WZ production in association with radiation of two jets (SM WZ QCD) was simulated using MADGRAPH [3]. MADGRAPH 5.1.5.10 was used to generate SM and non-SM VBS WZ events.

3.1 Event Selection

After PYTHIA 6.4 [10] parton showering, additional detector effects are applied using DELPHES 3.0.9 [11] with the Snowmass parameterization [6, 7, 8]. Events are considered VBS WZ candidates provided they meet the following criteria:

- Exactly three selected leptons (each with $p_T > 25$ GeV) which can be separated into an opposite sign, same flavor pair and an additional single lepton
- At least two selected jets with $p_T > 50$ GeV
- $m_{jj} > 1$ TeV, where m_{jj} is the invariant mass of the two highest- p_T selected jets

3.2 Statistical Analysis

The statistical analysis is identical to that employed in Sec. 2.2. As with the VBS ZZ channel, we present sensitivity studies with and without the UV bound applied, to show the impact of the UV bound. The UV bounds for different operators are shown in Figure 5. We present the 5σ -significance discovery values and 95% CL limits in

Table 2. Figure 8 shows the signal significance as a function of f_{T1}/Λ^4 and $c_{\phi d}/\Lambda^2$ without the UV bound and the corresponding reconstructed 4-lepton invariant mass distributions are shown in Figure 6. The same distributions with the UV bounds are shown in Figure 7.

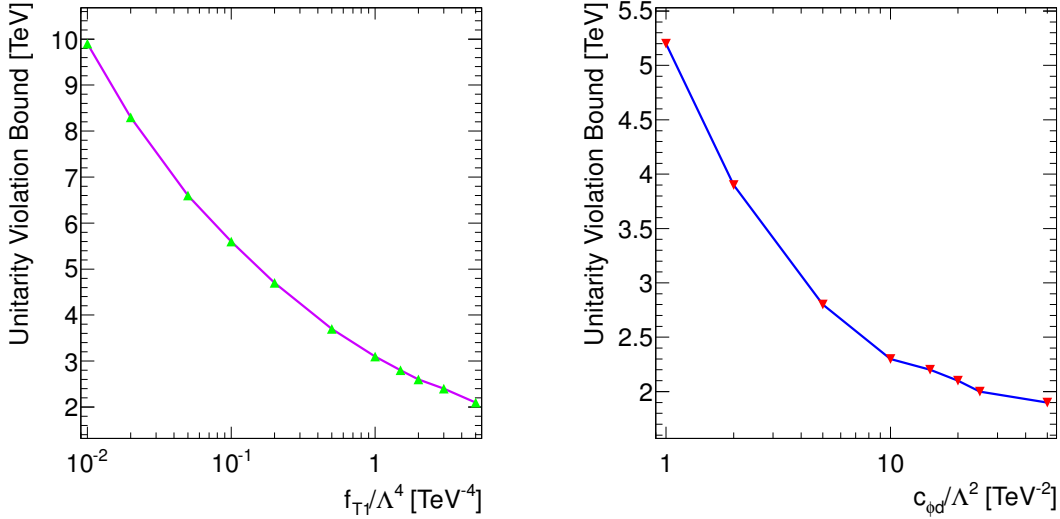


Figure 5: The unitarity violation bounds for the dimension-8 operator $\mathcal{L}_{T,1}$ (left) and the dimension-6 operator $\mathcal{L}_{\phi d}$ (right) are shown as functions of operator coefficient values in $pp \rightarrow WZ + 2j \rightarrow \ell\nu\ell\ell + 2j$ processes.

Parameter	Luminosity [fb ⁻¹]	14 TeV		33 TeV	
		5 σ	95% CL	5 σ	95% CL
$c_{\phi d}/\Lambda^2$ [TeV ⁻²]	3000	15.2 (15.2)	9.1 (9.1)	12.6 (12.7)	7.7 (7.7)
	300	28.5 (28.7)	17.1 (17.1)	23.1 (23.3)	14.1 (14.2)
f_{T1}/Λ^4 [TeV ⁻⁴]	3000	0.6 (0.9)	0.4 (0.5)	0.3 (0.6)	0.2 (0.3)
	300	1.1 (1.6)	0.7 (1.0)	0.6 (0.9)	0.3 (0.6)

Table 2: In $pp \rightarrow WZ + 2j \rightarrow \ell\nu\ell\ell + 2j$ processes, 5 σ -significance discovery values and 95% CL limits are shown for coefficients of higher-dimension operators with 300 fb⁻¹/3000 fb⁻¹ of integrated luminosity at $\sqrt{s} = 14$ TeV and $\sqrt{s} = 33$ TeV. The results obtained after applying the UV bounds are shown in parentheses.

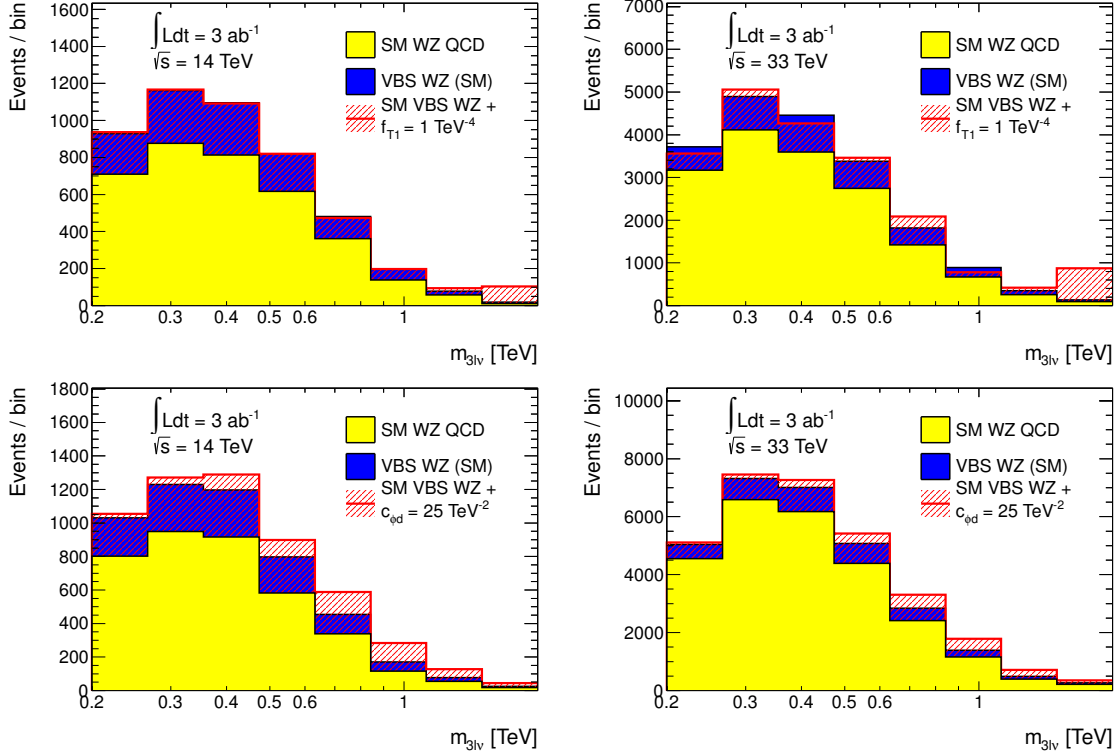


Figure 6: In the $pp \rightarrow WZ + 2j \rightarrow l\nu ll + 2j$ channel, the reconstructed WZ mass spectrum comparisons between Standard Model and dimension-8 operator coefficient $f_{T1}/\Lambda^4 = 1 \text{ TeV}^{-4}$ (top) and dimension-6 operator coefficient $c_{\phi d}/\Lambda^2 = 25 \text{ TeV}^{-2}$ (bottom) are shown using the charged leptons and the neutrino solution after requiring $m_{jj} > 1 \text{ TeV}$ at $\sqrt{s} = 14 \text{ TeV}$ (left) and 33 TeV (right). The overflow and underflow bins are included in the plots. The UV bounds have not been applied.

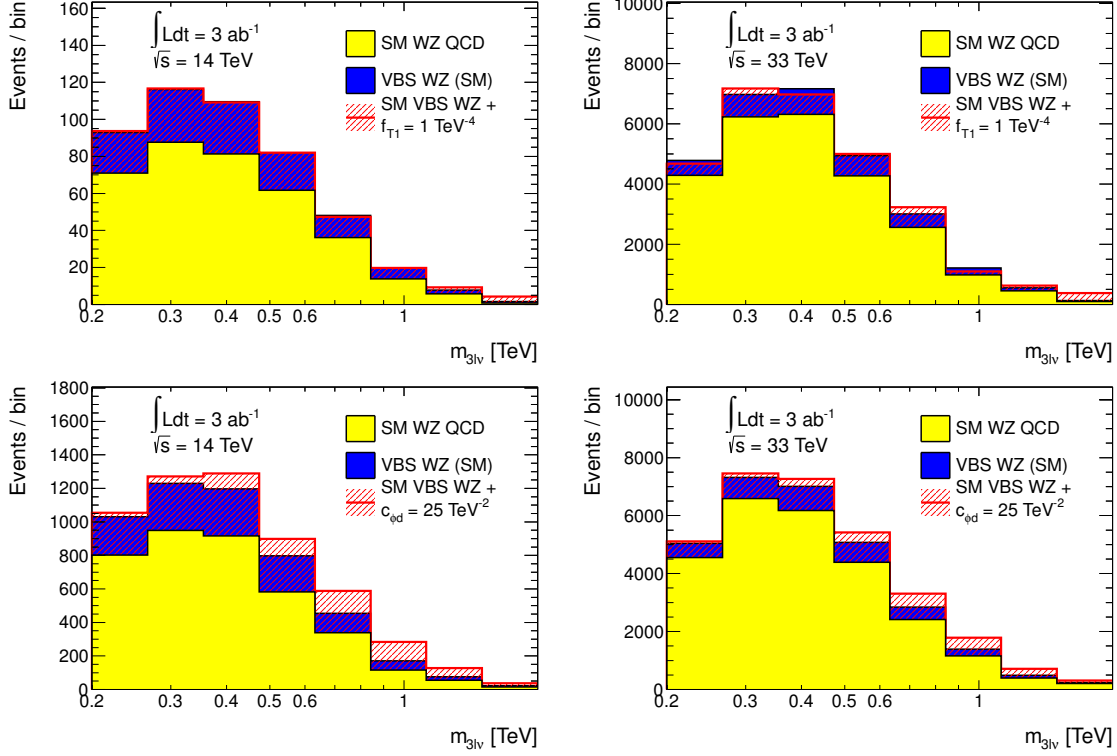


Figure 7: In the $pp \rightarrow WZ + 2j \rightarrow \ell\nu\ell\ell + 2j$ channel, the reconstructed WZ mass spectrum comparisons between dimension-8 operator coefficient $f_{T1}/\Lambda^4 = 1 \text{ TeV}^{-4}$ (top), dimension-6 operator coefficient $c_{\phi d}/\Lambda^2 = 25 \text{ TeV}^{-2}$ (bottom) and Standard Model are shown using the charged leptons and the neutrino solution after requiring $m_{jj} > 1 \text{ TeV}$ at $\sqrt{s} = 14 \text{ TeV}$ (left) and 33 TeV (right). The overflow and underflow bins are included in the plots. The UV bounds have been applied.

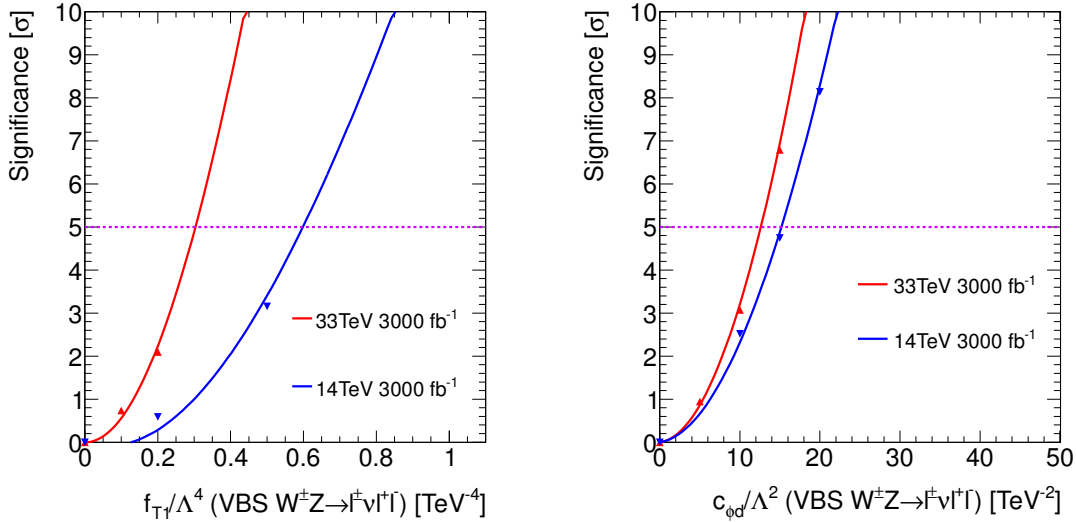


Figure 8: $pp \rightarrow WZ + 2j \rightarrow \ell\nu\ell\ell + 2j$ signal significance as a function of f_{T1}/Λ^4 (left) and $c_{\phi d}/\Lambda^2$ (right) calculated from reconstructed WZ mass spectra at $\sqrt{s} = 14 \text{ TeV}$ and 33 TeV . The UV bounds have not been applied.

4 VBS $W^\pm W^\pm \rightarrow \ell\nu\ell\nu$

The sensitivity to new physics was examined in the $pp \rightarrow W^\pm W^\pm + 2j \rightarrow \ell^\pm \nu \ell^\pm \nu + 2j$ (ssWW) channel where ℓ is an electron or muon. The dimension-8 operator $\mathcal{L}_{T,1}$ as shown in Eqn. 4, was used to probe deviations from SM predictions. This operator causes the strongest enhancement of the ssWW VBS cross section relative to the SM value. Table 3 shows the relative cross section yield due to each operator relevant to ssWW production.

operator	cross section ratio
$\mathcal{L}_{S,0}$	1.1
$\mathcal{L}_{S,1}$	1.0
$\mathcal{L}_{M,0}$	1.3
$\mathcal{L}_{M,1}$	1.1
$\mathcal{L}_{T,0}$	33
$\mathcal{L}_{T,1}$	150
$\mathcal{L}_{T,2}$	17

Table 3: Ratio of cross sections due to each dimension-8 operator with respect to the Standard Model value, for operator coefficients $f/\Lambda^4 = 10 \text{ TeV}^{-4}$ for VBS ssWW production at the LHC with $\sqrt{s} = 14 \text{ TeV}$. The SM cross section is 9 fb.

A range of coefficient values with sensitivities near the 5σ significance level were studied for 14 TeV and 100 TeV pp machine scenarios for various pileup conditions. The effect of a UV bound was also considered.

4.1 Monte Carlo Predictions

The samples were generated using MADGRAPH version 5.1.5.11 [3] for backgrounds, SM VBS, and new physics. The main backgrounds in ssWW VBS production are ssWW QCD diagrams, WZ , $W\gamma$, and mis-identification backgrounds including charge mis-identification. Following [15], the $W\gamma$ and mis-identification backgrounds were assumed to have the same shape as the WZ background and therefore, the WZ background was scaled appropriately (by a factor of 2) to account for these other backgrounds as well.

4.2 Event Selection

After PYTHIA 6.4 [10] parton showering, additional detector effects are applied using DELPHES 3.0.9 [11] with the Snowmass parameterization [6, 7, 8]. The analysis selection of the VBS ssWW candidates were given by the following criteria:

- Exactly two leptons of same sign each with $p_T > 25 \text{ GeV}$
- At least two jets with $p_T > 50 \text{ GeV}$
- $m_{jj} > 1 \text{ TeV}$, where m_{jj} is the invariant mass of the two highest- p_T jets

The high jet p_T cut helps protect against pileup jets while the m_{jj} cut strongly selects for the VBS signal region.

The UV bound for each f_{T1}/Λ^4 value used for this channel is shown in Fig. 9.

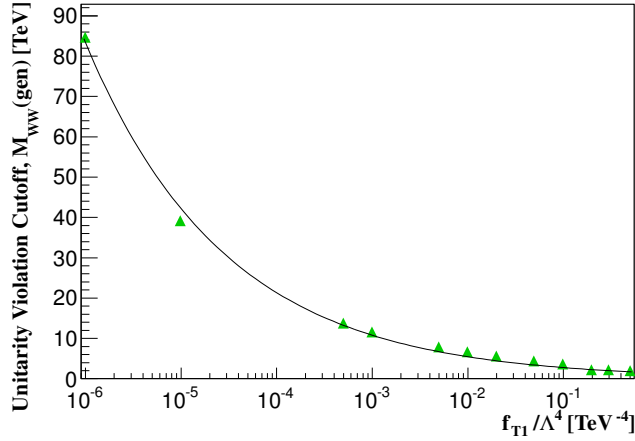


Figure 9: The Unitarity Violation (UV) cut-off values for a given f_{T1}/Λ^4 value for the VBS ssWW final state.

4.3 Statistical Analysis

Following [14, 15], the 4-body invariant mass of the two leading jets and the two leptons, m_{jjll} , was used to discriminate new physics from the SM. The statistical analysis approach is identical to that in Sec. 2.2.

Figure 10 compares the shape of the m_{jjll} distributions for the SM and two values of f_{T1}/Λ^4 (0.1 TeV^{-4} and 0.2 TeV^{-4} , respectively) at 14 TeV. Increasing the anomalous quartic coupling increases the event rate at the high end of the m_{jjll} spectrum. A similar plot for 100 TeV is shown in Figure 11 for $f_{T1}/\Lambda^4 = 0.001 \text{ TeV}^{-4}$.

The different pileup scenarios as well as the effect of the UV bound are shown in Figure 12 for different pp collider energies. The pileup has a small, but non-negligible effect whereas the UV bound has a larger effect. The significance values reported in Table 4 are without the UV bound applied and with the UV cut-off in parentheses.

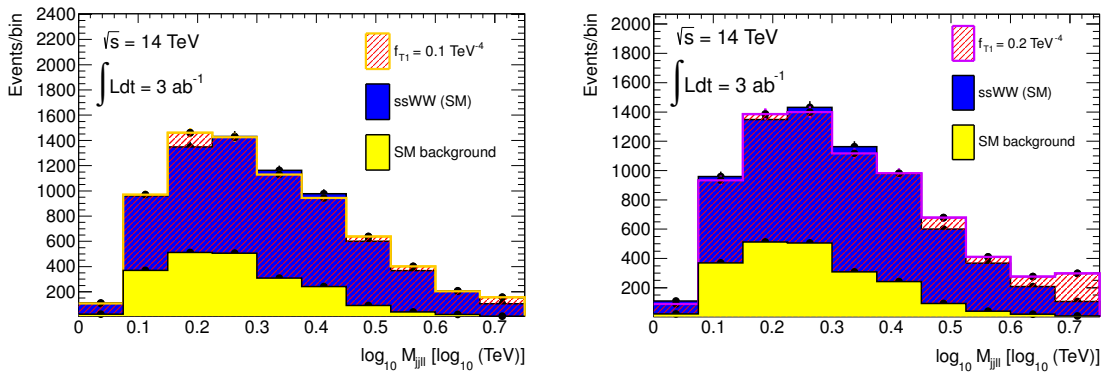


Figure 10: The invariant mass of the 4-body m_{jjll} system in ssWW events is shown for f_{T1}/Λ^4 equal to 0.1 TeV^{-4} corresponding to a significance of 4.2σ (left) and $f_{T1}/\Lambda^4 = 0.2 \text{ TeV}^{-4}$ with 17σ significance (right) for $\sqrt{s} = 14 \text{ TeV}$, 140 pileup events per crossing, without the UV cut-off applied, and 3000 fb^{-1} scenario.

A summary of the 5σ significance and the 95% Confidence Level (CL) for each machine scenario is listed in Table 4 along with a direct comparison of 14 TeV and

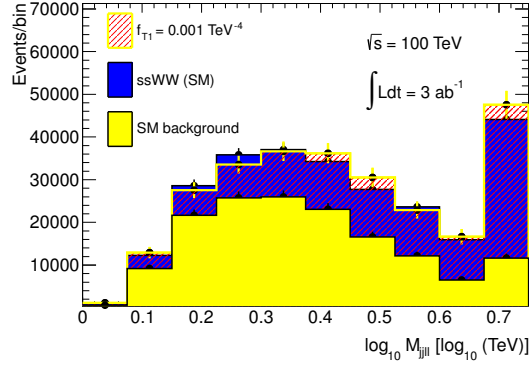


Figure 11: In ssWW events, m_{jj} for $f_{T1}/\Lambda^4 = 0.001$ corresponding to a 4σ significance for the case of a $\sqrt{s} = 100$ TeV pp machine with 263 pileup, without the UV cut-off applied, at 3000 fb^{-1} is shown.

100 TeV machines at 3000 fb^{-1} for zero pileup. At 14 TeV, by accumulating 3000 fb^{-1} compared to 300 fb^{-1} , the sensitivity to f_{T1}/Λ^4 is improved by a factor of two. Comparing a 14 TeV machine to a 100 TeV machine, we obtain at least a factor of 100 gain in sensitivity to the operator coefficient f_{T1}/Λ^4 for a 5σ discovery value.

Parameter	\sqrt{s} [TeV]	Luminosity [fb^{-1}]	pileup	5σ [TeV^{-4}]	95% CL [TeV^{-4}]
f_{T1}/Λ^4	14	300	50	0.2 (0.4)	0.1 (0.2)
f_{T1}/Λ^4	14	3000	140	0.1 (0.2)	0.06 (0.1)
f_{T1}/Λ^4	14	3000	0	0.1 (0.2)	0.06 (0.1)
f_{T1}/Λ^4	100	1000	40	0.001 (0.001)	0.0004 (0.0004)
f_{T1}/Λ^4	100	3000	263	0.001 (0.001)	0.0008 (0.0008)
f_{T1}/Λ^4	100	3000	0	0.001 (0.001)	0.0008 (0.0008)

Table 4: In $pp \rightarrow W^\pm W^\pm + 2j \rightarrow \ell\nu\ell\nu + 2j$ processes, 5σ -significance discovery values and 95% CL limits are shown for coefficients of the higher-dimension operator, f_{T1}/Λ^4 , for different machine scenarios without the UV cut and with the UV cut in parentheses. Pileup refers to the number of pp interactions per crossing.

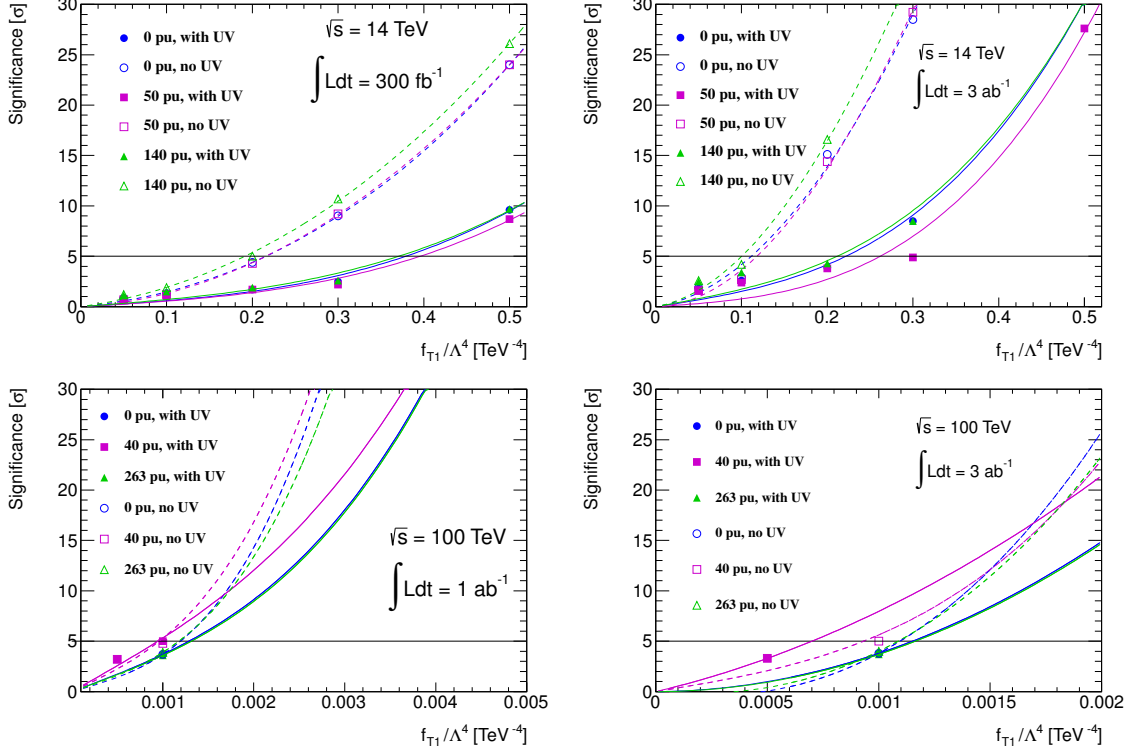


Figure 12: The significance trends for each beam energy and luminosity are shown for the various pileup scenarios. The fits are done with a 3rd order polynomial (curves). For the each set of machine conditions, each pileup scenario was considered with (solid points/solid curves) and without (open points/dashed curves) the UV bound. The top row displays the $\sqrt{s} = 14$ TeV cases at 300 fb⁻¹ (left) and 3000 fb⁻¹ (right). The bottom row shows the $\sqrt{s} = 100$ TeV cases at 1000 fb⁻¹ (left) and 3000 fb⁻¹ (right).

5 $WWW \rightarrow \ell\nu\ell\nu\ell\nu$

In the Standard Model (SM), the only allowed quartic coupling terms in the Lagrangian are $WWWW$, $WWZZ$, $WWZ\gamma$ and $WW\gamma\gamma$, and they are completely specified. Measuring these couplings will provide stringent tests on the SM and guide searches on physics beyond the SM. These couplings can be measured using triboson production as well as vector boson scattering. The triboson WWW production probes the $WWWW$ coupling, while WWZ and $WW\gamma$ production probe the $WWZZ$, $WWZ\gamma$ and $WW\gamma\gamma$ couplings, respectively [16, 17]. This section describes a cross section scan of WWW , WWZ , WZZ and ZZZ production for different anomalous couplings induced by higher-dimension operators, followed by a case study of WWW production for both dimension-8 and dimension-6 operators.

The dimension-8 operator studied most extensively was the $\mathcal{L}_{T,0}$ operator, given below

$$\mathcal{L}_{T,0} = \frac{f_{T0}}{\Lambda^4} \text{Tr}[\hat{W}_{\mu\nu}\hat{W}^{\mu\nu}] \times \text{Tr}[\hat{W}_{\alpha\beta}\hat{W}^{\alpha\beta}] \quad (6)$$

The dimension-6 operator used is \mathcal{L}_{WWW} , given below

$$\mathcal{L}_{WWW} = \frac{c_{WWW}}{\Lambda^2} \text{Tr}[W_{\mu\nu}W^{\nu\rho}W_{\rho}^{\mu}] . \quad (7)$$

5.1 Monte Carlo Predictions

MADGRAPH 5.1.5.11 [3] was used to generate all WWW signal and SM samples and the background samples. In all cases W and Z bosons were required to decay leptonically to electrons or muons. Default generator-level cuts on the leptons were $p_T > 10$ GeV and $|\eta| < 2.5$.

We performed a cross section scan to compare the SM cross sections to anomalous coupling cross sections for various higher-dimension operators (Tables 5 and 6). From the study, the $\mathcal{L}_{T,0}$ operator is found to have the largest effect on triboson production from the dimension-8 operators, and \mathcal{L}_{WWW} from the dimension-6 operators, particularly in the WWW channel. For this reason, we focus on this channel and these operators for the remainder of this section.

5.2 Event Selection

After PYTHIA 6.4 [10] parton showering, additional detector effects are applied using DELPHES 3.0.9 [11] with the Snowmass parameterization [6, 7, 8]. This parameterization includes effects from pile-up events. We have studied these effects and found them to be negligible for this analysis, which focuses on events with high invariant mass of the triboson system. Thus, all results presented in this section are extracted using Monte Carlo events generated without pile-up in the interest of reducing computational time.

Events are considered to be part of the WWW signal if they meet the following criteria, where $p_T(\ell)$ is the transverse momentum of the lepton, $M(\text{all lep})$ is the invariant mass of all the charged leptons with $p_T(\ell) > 25$ GeV and E_T^{miss} is the missing transverse energy of the event:

- At least three leptons, where leptons must have $p_T(\ell) > 25$ GeV

operator	WWW	WWZ	WZZ	ZZZ
SM cross section [ab]	603	124	9.63	0.972
$\mathcal{L}_{S,0}/\text{SM}$	1.0	1.0	1.0	1.0
$\mathcal{L}_{S,1}/\text{SM}$	1.0	1.0	1.0	1.0
$\mathcal{L}_{M,0}/\text{SM}$	1.46	1.09	1.05	1.02
$\mathcal{L}_{M,1}/\text{SM}$	1.17	1.02	1.04	1.03
$\mathcal{L}_{M,2}/\text{SM}$	1.0	1.05	1.0	1.02
$\mathcal{L}_{M,3}/\text{SM}$	1.0	1.01	1.00	1.01
$\mathcal{L}_{T,0}/\text{SM}$	18.31	3.96	3.38	2.90
$\mathcal{L}_{T,1}/\text{SM}$	15.15	2.10	2.83	2.90
$\mathcal{L}_{T,2}/\text{SM}$	4.48	1.32	1.35	1.54
$\mathcal{L}_{T,8}/\text{SM}$	1.0	1.0	1.0	1.31
$\mathcal{L}_{T,9}/\text{SM}$	1.0	1.0	1.0	1.08

Table 5: The ratios of cross sections for various dimension-8 operators to SM values are shown for a $\sqrt{s} = 14$ TeV pp collider. In each case, the coefficient of the dimension-8 operator was set to 10 TeV^{-4} . All channels are fully leptonic decays.

operator	WWW	WWZ	WZZ	ZZZ
SM cross section [ab]	603	124	9.63	0.972
$\mathcal{L}_{WWW}/\text{SM}$	1.4	1.3	1.4	1.0
\mathcal{L}_W/SM	1.1	1.1	1.2	1.1
\mathcal{L}_b/SM	1.0	1.0	1.0	1.0

Table 6: The ratios of cross sections for various dimension-6 operators to SM values are shown for a $\sqrt{s} = 14$ TeV pp collider. In each case, the coefficient of the dimension-6 operator was set to 5 TeV^{-2} . All channels are fully leptonic decays.

- No two leptons may have the same flavor and opposite charge (to suppress diboson WZ background)
- $M(\text{all lep}) > 400 \text{ GeV}$
- $E_T^{\text{miss}} > 150 \text{ GeV}$

These selections were specifically chosen to optimize the signal and reduce backgrounds. The backgrounds considered include Z +jets, W +2 jets, $t\bar{t}$, diboson (WW , WZ , ZZ), and $Z + \gamma$. The first selection reduces particularly the W +jets, Z +jets and WW backgrounds, and the second reduces backgrounds with Z bosons. The selection on lepton number also helps to reduce the $t\bar{t}$ background, but as only one jet has to fake a lepton and the cross-section for this process is much higher than the signal process, we still have a comparatively large contribution from $t\bar{t}$ production. The last two selections help to reduce this remaining $t\bar{t}$ contamination. After these selections, the results are not significantly affected by the remaining background events and these background processes are neglected in the final analysis.

There is an additional selection at the parton (truth) level to remove events in the kinematic region where the anomalous coupling amplitude would violate unitarity. Events are removed if the invariant mass of the three W bosons is larger than the UV bound. These bounds are estimated using the form factor tool available with VBFNLO [12] and are presented for various values of f_{T0}/Λ^4 and c_{WW}/Λ^2 in Figure 13. The bound rises rapidly for lower values of these coefficients, leading to a reduced impact of this bound. Conversely, for higher values of the coefficients, where the cross-section is higher, the impact of this bound is stronger.

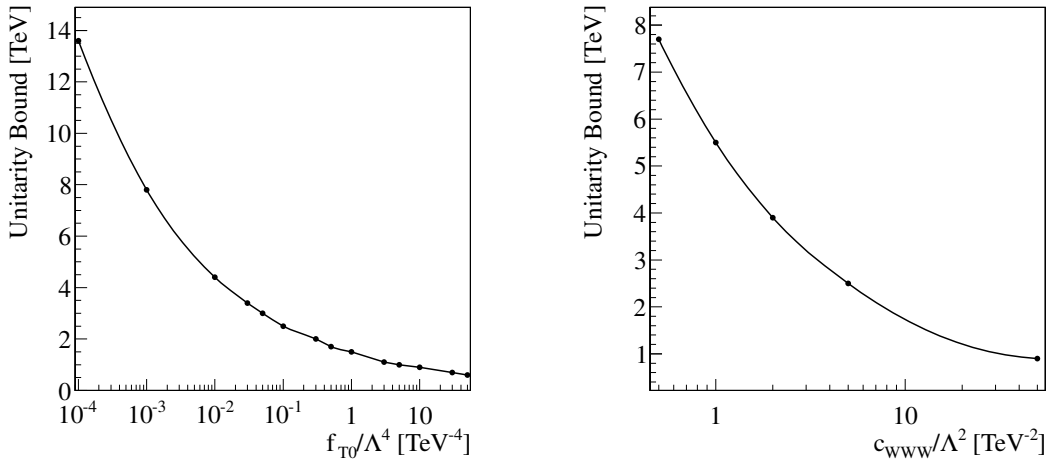


Figure 13: Unitarity bounds for the $\mathcal{L}_{T,0}$ operator (left) and for the \mathcal{L}_{WW} operator (right) are shown in various scenarios.

In the next section, for both $\mathcal{L}_{T,0}$ and \mathcal{L}_{WW} operators, we present results without the UV bound applied. We also comment on expectations with the application of the UV bound in Sec. 5.3.1.

5.3 Statistical Analysis

The distribution of $M(\text{all lep})$ is used for hypothesis testing. We compare the standard model prediction with the prediction for a non-zero value of a given higher-dimension operator. The statistical analysis is identical to that employed in Sec. 2.2. Figure 16 shows the WWW templates used for the $\sqrt{s} = 33$ TeV pp collider, before the lepton invariant mass selection. The significance estimate uses distributions with this cut applied and different binning depending on the collider energy. The fits of the significance curves use quadratic functions except for the 100 TeV and 33 TeV c_{WWW} curves without (with) the application of the UV bound, which are fit better by an exponential function (a third-order polynomial). Figure 15 shows the significance estimates for various f_{T0} and c_{WWW} values for different hadron collider machines being studied for Snowmass. As the machine energies and integrated luminosities increase we are able to put tighter constraints on these operators, and of course we are also able to discover and probe new physics at increasingly higher mass scales and/or smaller couplings.

Parameter	dim.	Luminosity [fb^{-1}]	14 TeV	33 TeV	100 TeV
c_{WWW}/Λ^2 [TeV^{-2}]	6	300	4.8 (8)	-	-
		1000	-	-	1.3 (1.5)
		3000	2.3 (2.5)	1.7 (2.0)	0.9 (1.0)
f_{T0}/Λ^4 [TeV^{-4}]	8	300	1.2	-	-
		1000	-	-	0.004
		3000	0.6	0.05	0.002

Table 7: In the $pp \rightarrow WWW \rightarrow 3\ell + 3\nu$ process, the 5σ -significance discovery values are shown for the coefficients of higher-dimension operators. The values in parentheses are obtained with the UV bound applied. pp colliders at $\sqrt{s} = 14, 33$ and 100 TeV are studied.

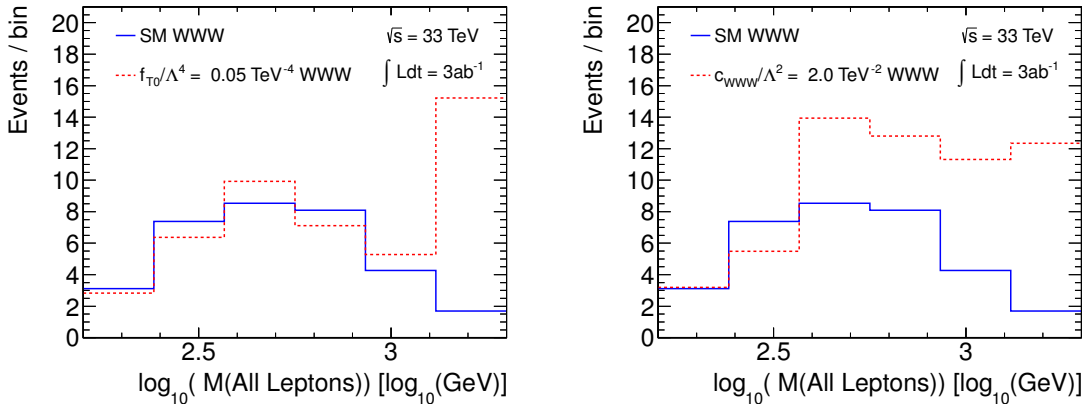


Figure 14: The invariant mass of all leptons is shown without applying the UV bound, for the SM and with $f_{T0}/\Lambda^4 = 0.05$ TeV^{-4} (left) and $c_{WWW}/\Lambda^2 = 2$ TeV^{-2} (right) for $\sqrt{s} = 33$ TeV. These distributions were made without the lepton invariant mass selection.

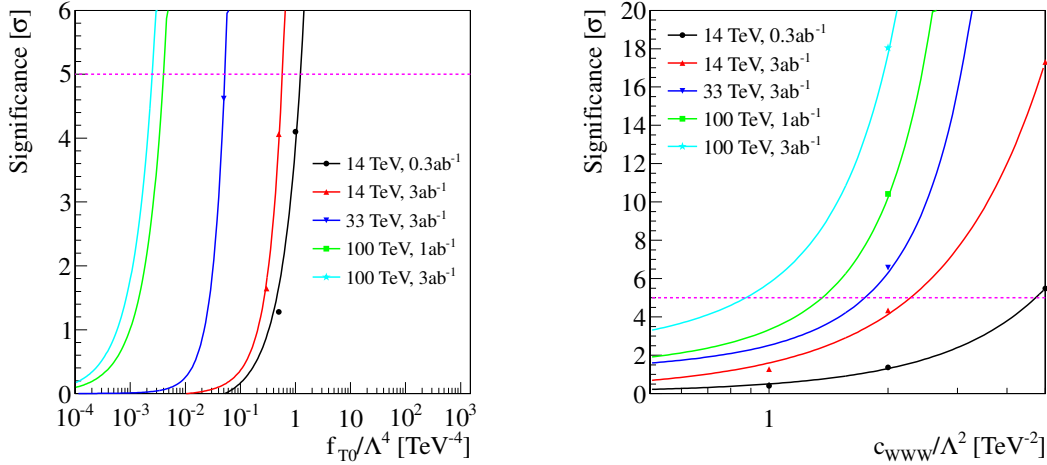


Figure 15: Significance values without the application of the UV bound as a function of f_{T0}/Λ^4 (left) and c_{WWW}/Λ^2 (right) are shown in various scenarios.

5.3.1 Impact of the Unitarity Violation Selection

As mentioned previously, we want to consider what happens when a UV bound is applied, which can be done in different ways. Here, we apply a selection on the generator-level WWW mass using the values discussed in Section 5.2 as an upper bound. Figure 16 shows the WWW templates used for the 33 TeV pp collider, before the lepton invariant mass selection was applied, with and without the UV bound applied for a given value of the $\mathcal{L}_{T,0}$ coefficient. The application of the UV bound lowers the expected number of signal events in the highest-mass bin. The UV bound used in this study has a large impact on the $\mathcal{L}_{T,0}$ results with this simple event removal, increasing the values from Table 7 of f_{T0}/Λ^4 at which we might expect a 5σ -significance discovery by more than a factor of 20. The large impact of the UV bound on the significance indicates that the breakdown of the EFT is imminent, and this channel is sensitive to the direct production of new particles which have been integrated out in the EFT for this dimension-8 operator. We expect this conclusion to be generically true for triboson production induced by dimension-8 operators, where the growth of the cross section with energy is more rapid than with dimension-6 operators.

The impact of applying the UV bound is less severe for the \mathcal{L}_{WWW} operator. Figure 17 shows the WWW templates used for the 33 TeV machine, before the lepton invariant mass selection for the same operator and coefficient, with and without the UV bound applied. There are fewer events in the last bins of Figure 17 due to the application of the UV bound, but overall the distributions are relatively similar, much more so than for $\mathcal{L}_{T,0}$ operator (see Figure 16). Figure 18 shows the significance estimates for various c_{WWW}/Λ^2 values for the different hadron collider machines being studied for Snowmass, with the UV bound applied. These values are generally 10-20% higher than the values of c_{WWW}/Λ^2 at which we might expect a 5σ -significance discovery without the removal of the high-mass events. As mentioned in the previous

paragraph, the dimension-6 operator amplitude does not violate unitarity as rapidly as a dimension-8 operator, when the energy is raised.

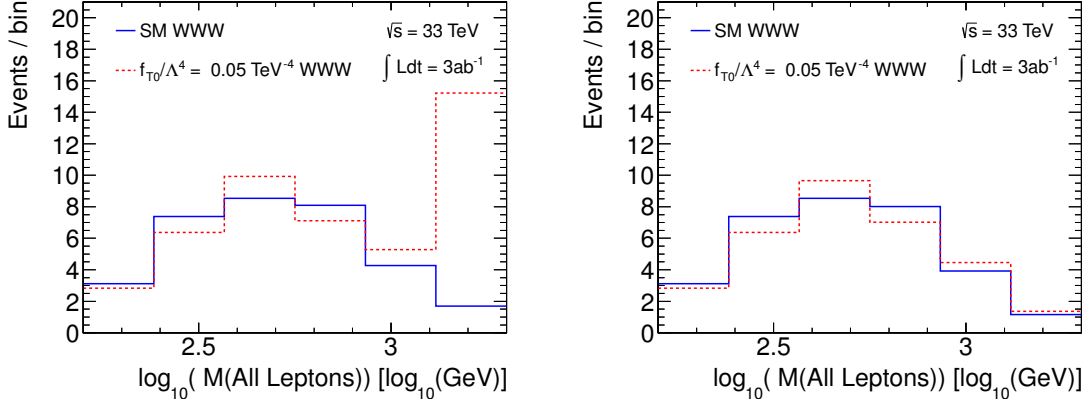


Figure 16: The invariant mass of all leptons is shown for the SM WWW process and with $f_{T0}/\Lambda^4 = 0.05 \text{ TeV}^{-4}$ for $\sqrt{s} = 33 \text{ TeV}$ without the UV bound (left) and with this bound applied (right). This distribution was made without the lepton invariant mass selection.

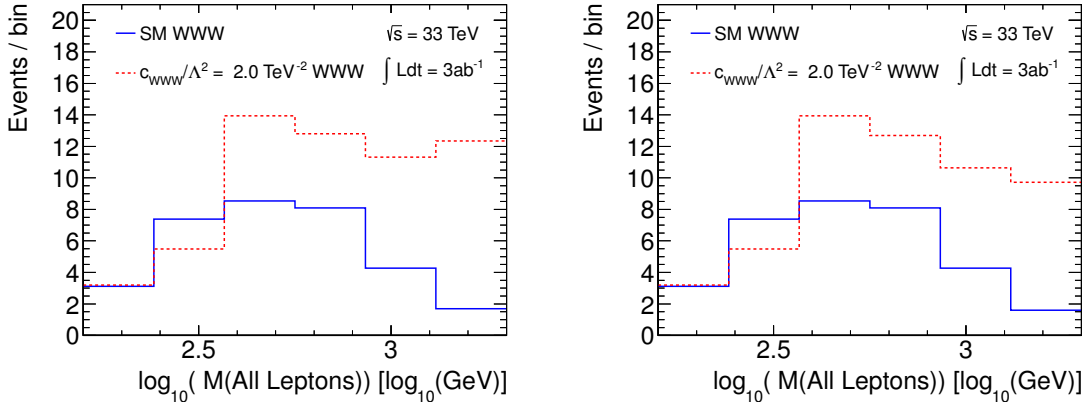


Figure 17: The invariant mass of all leptons is shown for the SM WWW process and with $c_{WWW}/\Lambda^2 = 2 \text{ TeV}^{-2}$ for $\sqrt{s} = 33 \text{ TeV}$ without the UV bound (left) and with this bound applied (right). This distribution was made without the lepton invariant mass selection.

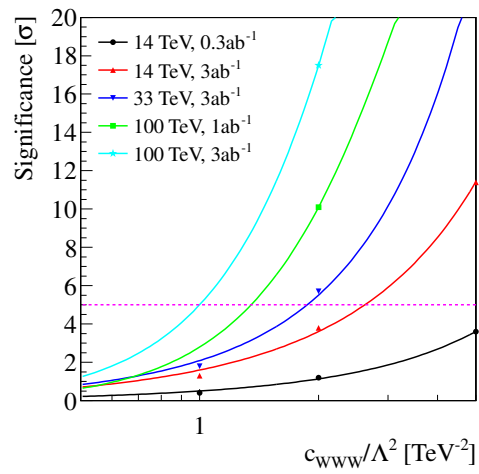


Figure 18: Significance values for the \mathcal{L}_{WW} operator coefficient are shown in various scenarios. The UV bound has been applied for these results.

6 $Z\gamma\gamma \rightarrow l^+l^-\gamma\gamma$

The $Z\gamma\gamma$ mass spectrum at high mass is sensitive to BSM triboson contributions. The lepton-photon channel allows full reconstruction of the final state and the calculation of the $Z\gamma\gamma$ invariant mass $m_{Z\gamma\gamma}$. We parameterize the BSM physics using the following operators

$$\mathcal{L}_{M,0} = \frac{f_{M0}}{\Lambda^4} \text{Tr}[\hat{W}_{\mu\nu}\hat{W}^{\mu\nu}] \times [(D_\beta\phi)^\dagger D^\beta\phi] \quad (8)$$

$$\mathcal{L}_{M,1} = \frac{f_{M1}}{\Lambda^4} \text{Tr}[\hat{W}_{\mu\nu}\hat{W}^{\nu\beta}] \times [(D_\beta\phi)^\dagger D^\mu\phi] \quad (9)$$

$$\mathcal{L}_{M,2} = \frac{f_{M2}}{\Lambda^4} [B_{\mu\nu}B^{\mu\nu}] \times [(D_\beta\phi)^\dagger D^\beta\phi] \quad (10)$$

$$\mathcal{L}_{M,3} = \frac{f_{M3}}{\Lambda^4} [B_{\mu\nu}B^{\nu\beta}] \times [(D_\beta\phi)^\dagger D^\mu\phi]. \quad (11)$$

They are selected because of the possibility to be converted to a_0 and a_C , the non-linear parametrization of anomalous couplings adopted by the LEP results.

MADGRAPH 5.1.5.10 [3] was used to generate all $Z\gamma\gamma$ samples and background samples, $Z\gamma j$ and Zjj . In all cases Z bosons were required to decay to electron or muon pairs.

6.1 Event Selection

After PYTHIA 6.4 [10] parton showering, the reconstruction effects of resolution and identification efficiency are applied using DELPHES [5, 6, 7, 8]. A constant jet-to-photon fake rate of 10^{-3} is applied to each jet in the $Z\gamma j$ and Zjj samples to construct smooth background templates. Events are considered $Z\gamma\gamma$ candidates provided they meet the following criteria:

- $p_T(\ell) > 25$ GeV, $|\eta(\ell)| < 2.0$
- $p_T(\gamma) > 25$ GeV, $|\eta(\gamma)| < 2.0$
- leading γ $p_T > 160$ GeV
- $|m_{\ell\ell} - 91$ GeV| < 10 GeV
- $\Delta R(\gamma, \gamma) > 0.4$; $\Delta R(\ell, \gamma) > 0.4$; $\Delta R(\ell, \ell) > 0.4$.

The $p_T > 160$ GeV requirement on the photon suppresses fake background. The 10 GeV invariant mass window cut around the Z boson mass peak suppresses the γ^* contribution to the dilepton system. The large angular separation (ΔR) between the photon and the lepton and the high transverse-momentum requirement of the photon reduces the final-state photon radiation contribution. This leads to the phase space which is uniquely sensitive to the quartic gauge coupling (QGC).

6.2 Statistical Analysis

The statistical analysis is identical to that employed in Sec. 2.2. The distribution of $m_{Z\gamma\gamma}$ is used for hypothesis testing. The dominant process in the QGC-sensitive kinematic phase space is $Z\gamma\gamma$ production while the fake backgrounds $Z\gamma j$ and Zjj are sub-dominant. We present sensitivity studies with and without the UV bound applied. The bounds for different operators are shown in Figure 19.

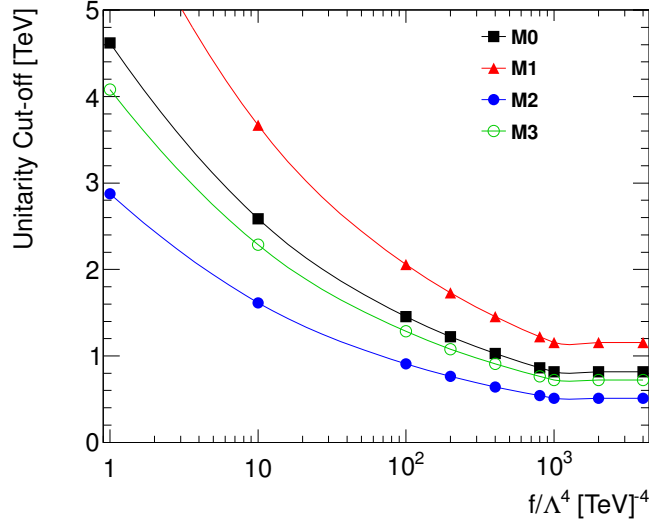


Figure 19: The unitarity violation bounds for $\mathcal{L}_{M,i}, i = 0\dots 3$ operators are shown as functions of their coefficient values in the $pp \rightarrow Z\gamma\gamma$ process.

Figure 20 shows the reconstructed 4-body invariant mass distribution for this channel at the $\sqrt{s} = 14$ TeV pp collider. The left upper figure shows the distributions without the UV bound. The other three plots show the mass distribution due to each anomalous QGC operator with the corresponding UV bound applied. The bound is applied as an additional event selection requirement on the 4-body mass.

To show the impact of the UV bound, we present the 5σ -significance discovery values and 95% CL limits both without (in parentheses) and with the UV bounds applied, in Table 8. Figure 21 shows the significance as function of coefficient values with the UV bound. The effect of UV cutoff is significant and as large as a factor of 5 – 10 for large coefficient values. The smaller the coefficient value, the smaller the UV cutoff effect.

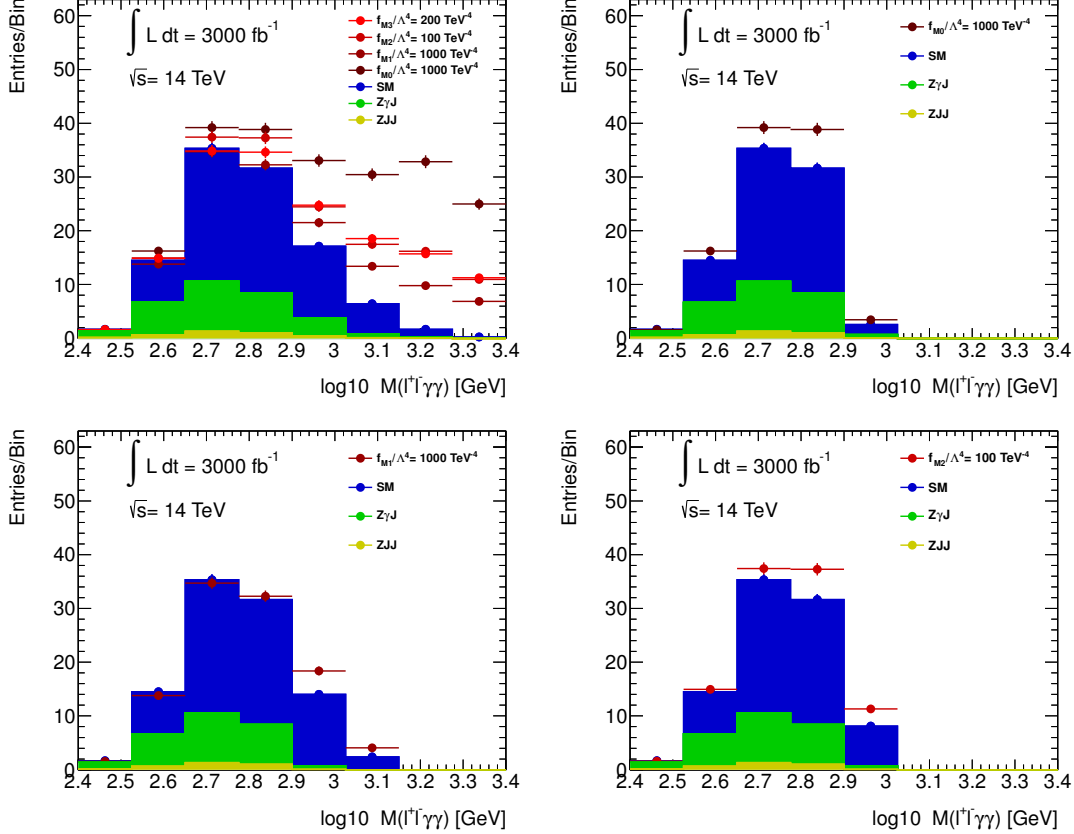


Figure 20: Reconstructed mass spectra using the charged leptons and photons after event selection are shown without the UV bound (top left) and with the UV bound (top right and bottom). The coefficient is selected to be near the 95% CL limit for each operator after applying the UV bound.

Parameter	\sqrt{s}	14 TeV	14 TeV	33 TeV	100 TeV
	Lum.	300 fb ⁻¹	3000 fb ⁻¹		
f_{M0}/Λ^4 [TeV ⁻⁴]	5 σ	7300 (830)	3600 (310)	1900 (190)	750 (120)
	95% CL	4200 (360)	1200 (160)	660 (120)	71 (59)
f_{M1}/Λ^4 [TeV ⁻⁴]	5 σ	7600 (1600)	3600 (680)	2100 (340)	1000 (220)
	95% CL	4500 (800)	1200 (290)	770 (160)	240 (126)
f_{M2}/Λ^4 [TeV ⁻⁴]	5 σ	3300 (130)	510 (48)	310 (26)	120 (16)
	95% CL	670 (56)	160 (21)	110 (13)	25 (10)
f_{M3}/Λ^4 [TeV ⁻⁴]	5 σ	2400 (250)	720 (120)	320 (66)	180 (34)
	95% CL	820 (133)	210 (52)	130 (23)	38 (15)

Table 8: In $pp \rightarrow Z\gamma\gamma \rightarrow l^+l^-\gamma\gamma$ processes, 5 σ -significance discovery values and 95% CL limits are shown for coefficients of dimension-8 operators with integrated luminosity of 300 fb⁻¹ at $\sqrt{s} = 14$ TeV and 3000 fb⁻¹ at $\sqrt{s} = 14$ TeV, 33 TeV and 100 TeV, respectively. To show the impact without the UV bound, the corresponding results are shown in parentheses.

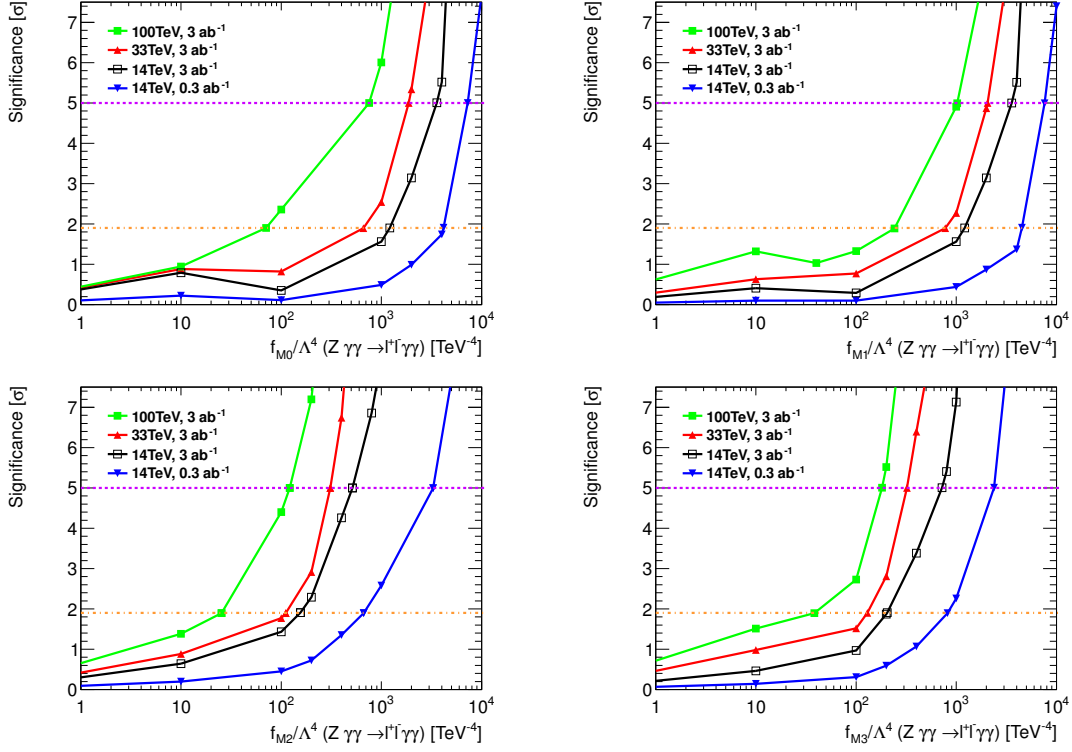


Figure 21: The signal significance as a function of f_{M_i}/Λ^4 , $i = 0,1,2,3$ with the UV bound applied, is shown for various collider options. The dashed lines indicate the 5σ and 95% CL limit values.

7 Conclusions

We have presented sensitivity studies for gauge-invariant dimension-6 and dimension-8 operators which can parameterize new physics involving Higgs and gauge boson fields. We have explored anomalous vector boson scattering and triboson production due to such operators at pp colliders with $\sqrt{s} = 14, 33$ and 100 TeV center-of-mass energy.

Our conclusions are as follows:

- The VBS ZZ final state, when used to probe the $\mathcal{L}_{\phi W}$ dimension-6 operator, increases in sensitivity to the operator coefficient by a factor of ≈ 1.9 when the luminosity is increased by a factor of 10 from 300 fb^{-1} to 3000 fb^{-1} , and by a factor of ≈ 1.2 when the collider energy is increased from 14 TeV to 33 TeV. When considering the dimension-8 operators $\mathcal{L}_{T,8}$ ($\mathcal{L}_{T,9}$), the sensitivity increases by a factor of 1.9 (1.5) due to the same luminosity increase and by a factor of ≈ 1.8 (1.5) due to the energy increase. The sensitivity to the dimension-6 operator is not affected by imposing a UV bound, while the sensitivity to the dimension-8 operator is reduced by a factor of about 1.8 when the bound is applied.
- The VBS WZ final state, when used to probe the $\mathcal{L}_{\phi d}$ dimension-6 operator, increases in sensitivity to the operator coefficient by a factor of ≈ 1.9 when the luminosity is increased from 300 fb^{-1} to 3000 fb^{-1} , and by a factor of ≈ 1.2 when the collider energy is increased from 14 TeV to 33 TeV. When considering the dimension-8 operator $\mathcal{L}_{T,1}$, the sensitivity increases by a factor of ≈ 1.8 due to the same luminosity increase and by a factor of ≈ 2 due to the energy increase. The sensitivity to the dimension-6 operator is not affected by imposing a UV bound, while the sensitivity to the dimension-8 operator is reduced by a factor of about 1.8 when the bound is applied.
- The VBS $ssWW$ final state, when used to probe the $\mathcal{L}_{T,1}$ dimension-8 operator, increases in sensitivity to the operator coefficient by a factor of ≈ 2 when the luminosity is increased from 300 fb^{-1} to 3000 fb^{-1} at $\sqrt{s} = 14$ TeV. An increase in collider energy from 14 TeV to 100 TeV increases the sensitivity by a factor of 100. The sensitivity is not affected at $\sqrt{s} = 100$ TeV by imposing a UV bound because the bound is very high for the value of the coefficient probed. The sensitivity at $\sqrt{s} = 14$ TeV is reduced by a factor of about 2 when the bound is applied.
- The triboson WWW final state, when used to probe the \mathcal{L}_{WWW} dimension-6 operator, increases in sensitivity to the operator coefficient by a factor of ≈ 2 when the luminosity is increased from 300 fb^{-1} to 3000 fb^{-1} at $\sqrt{s} = 14$ TeV. An increase in collider energy from 14 TeV to 33 TeV (100 TeV) increases the sensitivity by a factor of 1.3 (2.5). These results are affected at the 10% level by the application of the UV bound. When probing the dimension-8 operator $\mathcal{L}_{T,0}$, the sensitivity to the operator coefficient increases by a factor of ≈ 2 when the luminosity is increased from 300 fb^{-1} to 3000 fb^{-1} at $\sqrt{s} = 14$ TeV. An increase in collider energy from 14 TeV to 33 TeV (100 TeV) increases the sensitivity by a factor of 12 (300). This dramatic increase is tamed by the UV bound; we take

this as an indication that WWW triboson production is a sensitive channel for direct production of new particles as the collider energy is raised.

- The triboson $Z\gamma\gamma$ final state, when used to probe the $\mathcal{L}_{M,i}$ dimension-8 operators, increases in sensitivity to the operator coefficient by a factor of 2 – 6 (depending on the operator considered) when the luminosity is increased from 300 fb^{-1} to 3000 fb^{-1} at $\sqrt{s} = 14 \text{ TeV}$. An increase in collider energy from 14 TeV to 33 TeV (100 TeV) increases the sensitivity by a factor of ≈ 2 (4 to 5). These results are strongly affected by the application of the UV bound.

The sensitivity to pileup effects has been studied and it is found that, for the leptonic decay modes presented here, the results are not sensitive to pileup effects.

It is important to note that the sensitivities for the 33 TeV and 100 TeV colliders are based on analyses that have not been re-optimized for higher energy colliders; the analyses were optimized for 14 TeV only. Optimization of the analyses for higher collider energies is important and should be revisited in the future as it will lead to further improvements of the sensitivity to new physics at those machines. Furthermore, the sensitivity can be improved using multivariate techniques.

References

- [1] C. Degrande, N. Greiner, W. Kilian, O. Mattelaer, H. Mebane, T. Stelzer, S. Wilenbrock and C. Zhang, “Effective Field Theory: A Modern Approach to Anomalous Couplings (private communication)” arXiv:1205.4231 [hep-ph].
- [2] O. J. P. Eboli, M. C. Gonzalez-Garcia and J. K. Mizukoshi, “ $pp \rightarrow jje^\pm\mu^\mp\nu\nu$ and $jje^\pm\mu^\mp\nu\nu$ at $\mathcal{O}(\alpha_{em}^6)$ and $\mathcal{O}(\alpha_{em}^4\alpha_s^2)$ for the study of the quartic electroweak gauge boson vertex at CERN LHC”, Phys. Rev. D **74**, (2006) 073005 [hep-ph/0606118].
- [3] J. Alwall, M. Herquet, F. Maltoni, O. Mattelaer and T. Stelzer, “MadGraph 5 : Going Beyond”, JHEP **1106**, (2011) 128 arXiv:1106.0522 [hep-ph].
- [4] S. Kretzer, H.L. Lai, F.I. Olness, and W.K. Tung, “Cteq6 parton distributions with heavy quark mass effects”, Phys. Rev. D **69**, (2004)114005 [hep-ph/0307022].
- [5] S. Ovin, X. Rouby and V. Lemaitre, “DELPHES, a framework for fast simulation of a generic collider experiment”, arXiv:0903.2225 [hep-ph].
- [6] J. Anderson *et al.*, “Snowmass Energy Frontier Simulations”, arXiv:1309.1057 [hep-ex].
- [7] A. Avetisyan *et al.*, “Methods and Results for Standard Model Event Generation at $\sqrt{s} = 14$ TeV, 33 TeV and 100 TeV Proton Colliders (A Snowmass Whitepaper)”, arXiv:1308.1636 [hep-ex].
- [8] A. Avetisyan, “Snowmass Energy Frontier Simulations using the Open Science Grid (A Snowmass 2013 whitepaper)”, arXiv:1308.0843 [hep-ex].
- [9] ATLAS Collaboration, “Measurement of the total ZZ production cross section in proton-proton collisions at $\sqrt{s} = 8$ TeV in 20 fb^{-1} with the ATLAS detector”, ATLAS-CONF-2013-020, CERN, Geneva, March, 2013. <http://cds.cern.ch/record/1525555>.
- [10] T. Sjostrand, S. Mrenna and P.Z. Skands, “PYTHIA 6.4 physics and manual”, JHEP **0605**, (2006) 026 arXiv:0603175 [hep-ph].
- [11] J. de Favereau *et al.*, “DELPHES 3, A modular framework for fast simulation of a generic collider experiment”, arXiv:1307.6346 [hep-ex].
- [12] O. Schlimpert and B. Feigl, “VBFNLO Utility to Calculate Form Factors”, Karlsruhe Institut fur Technologie, <http://www.itp.kit.edu/~vbfneweb/wiki/doku.php?id=download:formfactor>.
- [13] ATLAS Collaboration, “A Measurement of WZ production in proton-proton collisions at $\sqrt{s} = 8$ TeV with the ATLAS detector”, ATLAS-CONF-2013-021, CERN, Geneva, March, 2013. <http://cds.cern.ch/record/1525557>.

- [14] ATLAS Collaboration, “Studies of Vector Boson Scattering with an Upgraded ATLAS Detector at a High-Luminosity LHC”, ATL-PHYS-PUB-2012-005, CERN, Geneva, Nov., 2012. <http://cds.cern.ch/record/1496527>.
- [15] ATLAS Collaboration, “Studies of Vector Boson Scattering And Triboson Production with an Upgraded ATLAS Detector at a High-Luminosity LHC”, ATL-PHYS-PUB-2013-006, CERN, Geneva, June, 2013. <http://cds.cern.ch/record/1558703>.
- [16] D. Green, “Vector Boson Fusion and Quartic Boson Couplings”, arXiv:0306160 [hep-ph].
- [17] A.S. Belyaev *et al.*, “Strongly Interacting Vector Bosons at the LHC: Quartic Anomalous Couplings”, arXiv:9805229 [hep-ph].

A Comparisons of $W^\pm Z$ and ZZ VBS cross sections at ILC and LHC

The following cross sections were computed with MADGRAPH at leading order for the VBS WZ and ZZ final states, inclusive of all decay channels.

coefficient (TeV^{-4})	Cross Section at LHC [fb]	Cross Section at ILC1000 [fb]
$f_{T0}/\Lambda^4 = 1$	612	13.6
$f_{T1}/\Lambda^4 = 1$	744	13.6
$f_{T2}/\Lambda^4 = 1$	553	13.6
$f_{M0}/\Lambda^4 = 1$	539	13.5
$f_{M1}/\Lambda^4 = 1$	536	13.6
$f_{M2}/\Lambda^4 = 1$	537	13.6
$f_{M3}/\Lambda^4 = 1$	539	13.5
$f_{S0}/\Lambda^4 = 1$	537	13.5
$f_{S1}/\Lambda^4 = 1$	534	13.5
Standard Model	537	13.6

Table 9: $pp \rightarrow WZ + 2j$ (LHC at $\sqrt{s} = 14$ TeV) and $e^+e^- \rightarrow WZ + 2j$ (ILC at $\sqrt{s} = 1$ TeV) Vector Boson Scattering cross section comparisons with dimension-8 operator coefficients.

coefficient (TeV^{-4})	Cross Section at LHC [fb]	Cross Section at ILC1000 [fb]
$f_{T0}/\Lambda^4 = 1$	327	0.808
$f_{T1}/\Lambda^4 = 1$	238	0.808
$f_{T2}/\Lambda^4 = 1$	159	0.784
$f_{T8}/\Lambda^4 = 1$	194	0.898
$f_{T9}/\Lambda^4 = 1$	144	0.824
$f_{M0}/\Lambda^4 = 1$	138	0.760
$f_{M1}/\Lambda^4 = 1$	134	0.768
$f_{M2}/\Lambda^4 = 1$	136	0.735
$f_{M3}/\Lambda^4 = 1$	133	0.790
$f_{S0}/\Lambda^4 = 1$	132	0.763
$f_{S1}/\Lambda^4 = 1$	133	0.763
Standard Model	133	0.765

Table 10: $pp \rightarrow ZZ + 2j$ (LHC at $\sqrt{s} = 14$ TeV) and $e^+e^- \rightarrow ZZ + 2j$ (ILC at $\sqrt{s} = 1$ TeV) Vector Boson Scattering cross section comparisons with dimension-8 operator coefficients.